Structural and electronic properties of transition-metal/$BaTiO_3$(001) interfaces

Fangyi Rao, Miyoung Kim, and A. J. Freeman
Department of Physics and Astronomy, Northwestern University, Evanston, Illinois 60208

Shaoping Tang and Mark Anthony
Texas Instruments, 13588 North Central Expressway 75243, P.O. Box 655934, MS 147, Dallas, Texas 75265

(Received 24 September 1996)

Electronic and structural properties of transition-metal/$BaTiO_3$(001) interfaces are studied by first-principles local-density full-potential linearized augmented plane-wave calculations with slab models. Equilibrium interlayer separations between metal overlayers (for the 5*d* metals Ta, W, Ir, and Pt) and the $BaTiO_3$ substrate are calculated by total-energy determinations. It is found that the preferred adsorption site for metal atoms on the $BaTiO_3$ surface is above the O site and the metal-oxygen distance increases from Ta to Pt while the binding energy decreases. Significant hybridization is found between metal *d* states and the O $2p-$Ti $3d$ states. The Fermi levels of the metals lie in the gap of $BaTiO_3$ and metal-induced gap states, as suggested by Heine's theory [Proc. Phys. Soc. London **81**, 300 (1962); Surf. Sci. **2**, 1 (1964); Phys. Rev. **138**, A1689 (1965)], are observed. The Schottky barrier in the interfaces is calculated by the position of E_F in the gap and the dependence of the barrier height on the metal work function is different from either Schottky and Mott's or Bardeen's [Phys. Rev. **71**, 717 (1947)] speculation. [S0163-1829(97)03316-X]

I. INTRODUCTION

In the past ten years, the scaling of the dynamic random access memory (DRAM) cell size has dramatically improved memory performance and chip density. It has been projected recently that the chip density will reach 256 Mb and 1 Gb levels in the 1998 and 2001 time frames, with the corresponding reduction in cell areas to 0.6 μm^2 and 0.24 μm^2, respectively.[1] Such high integration will require materials of high dielectric constants in order to be able to construct cells of sufficient capacitance in the reduced available area. With their high-permittivity, ferroelectric materials, such as barium strontium titanate (BST) and lead zirconate titanate (PZT), are considered good candidates for ultra-large-scale integration DRAM. Increased attention has been drawn to the electrical properties of their thin-film devices for potential DRAM applications.[2,3]

A ferroelectric memory cell capacitor is typically made by depositing metal layers as electrodes on top and bottom of the BST or PZT films. This simple device has two metal/ferroelectric interfaces and its electrical performance can be affected significantly by the interface properties and the materials selection for top and bottom electrodes. Indeed, experimental work suggests that the DRAM properties of metal-ferroelectric-metal capacitors strongly depend on the electrode properties as well as on the choice of the ferroelectric materials. For example, Chen and Kingon[4] used different metals for the top and bottom electrodes on PZT thin-film capacitors and observed that electric dc breakdown occurs at very different voltages for positive and negative polarities. This implies that it matters very much which metal the electron comes from that initiates breakdown in the PZT film. Equivalent experiments for BST with Pt, W, and Al as electrodes were reported by Scott *et al.*;[5] they also found large differences in breakdown field with polarity for unlike electrodes and no difference when the top and bottom are of the same metal. The dielectric constant of $SrTiO_3$ films thinner than 100 nm were studied by Abe and Komatsu[6] and the interface between the electrode and $SrTiO_3$ was found to cause the lowering of the dielectric constant. Kim *et al.*[7] have investigated the effects of electrode material on the electrical properties of ferroelectric capacitors by using Au, Pt, W, Ti, and TiN as top electrodes and Pt as the bottom electrode. They found that a PZT capacitor with metal electrodes has Schottky junctions between bulk PZT and both top and bottom electrodes. This results in asymmetrical ferroelectric hysteresis loops for capacitors with non-noble top (W, Ti, and TiN) electrodes. The internal bias values correlate well with the metal work-function difference between top and bottom electrode materials. Recent leakage current measurements on $SrTiO_3$ thin films by Dietz *et al.*[8] show that leakage current varies by orders of magnitude with different metals (Al, Ti, Pd, Pt, and Au) as electrodes.

To understand the effects of metal/ferroelectric interfaces on the performance of ferroelectric capacitors and make a successful device, the basic structural and electronic properties of the interfaces have to be investigated at the microscopic level. Recognizing that microscopic information about the interface is very hard to obtain from experiments, first-principles electronic-structure calculations have proven to be a powerful tool to compensate for this deficiency. In this paper, we present results of a first-principles study of the transition-metal/$BaTiO_3$(001) interfaces where the transition metals are the 5*d* metals Ta, W, Ir, and Pt. At this stage, no ferroelectric displacement of $BaTiO_3$ is considered in our calculations. We restrict ourselves to the nonferroelectric phase and focus on the interface properties. Stable structures are calculated by total-energy relaxation. Interface electronic structures (such as charge density and charge transfer), density of states, and band structures, are determined in order to understand the bonding mechanism and the interaction between the metals and the $BaTiO_3$ surface. In the last part of the paper, we calculate the Schottky barrier of metal/$BaTiO_3$ interfaces by determining the position of the Fermi level in the gap of $BaTiO_3$.

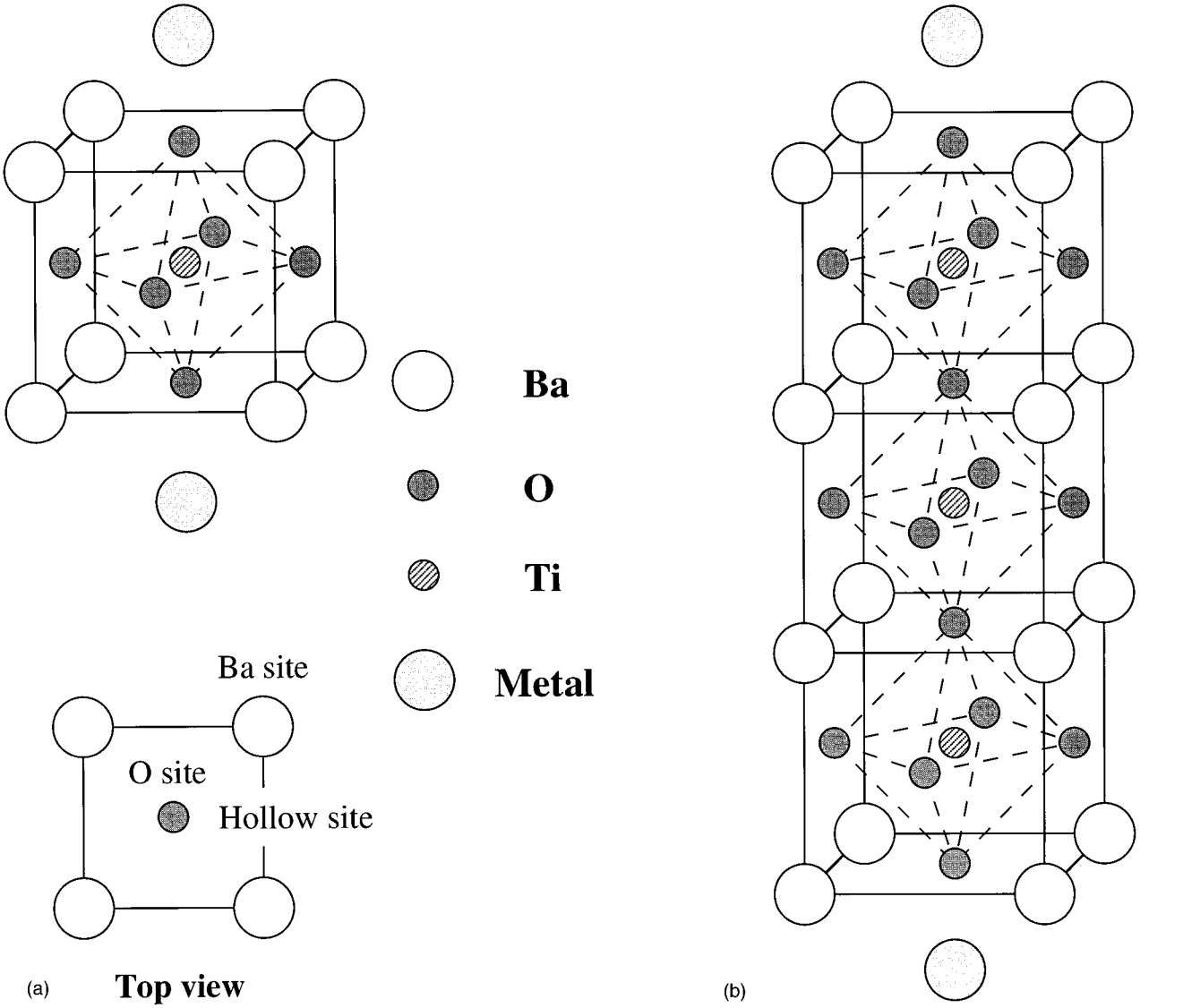

FIG. 1. Slab models of the Pt/$BaTiO_3$ interface used in the calculations: (a) the one-cell slab with top view of the $BaTiO_3$(001) surface and (b) the three-cell slab.

II. COMPUTATIONAL MODEL AND METHODOLOGY

$BaTiO_3$ has a cubic perovskite structure with Ti at the body center, O at face centers, and Ba at corners of the cubic. There are two possible surface planes for $BaTiO_3$ at the (001) direction: the BaO and TiO_2 planes and their interactions with the metal atom could be different. In this paper we only consider the BaO case, the TiO_2 case will be studied in the future. We set up two slab models to study the transition-metal/$BaTiO_3$(001) interfaces, which are displayed in Fig. 1. In the one-cell model, the $BaTiO_3$ slab consists of one fcc cell in the perpendicular direction, i.e., the z direction, with a metal monolayer adsorbed on the surface on each side of the slab. Thus the one-cell model has nine atoms per unit cell (two Ba, one Ti, four O, and two metal atoms). In the three-cell model, the $BaTiO_3$ slab consists of three fcc cells and the number of atoms per unit cell increases to 19 (four Ba, three Ti, ten O, and two metal atoms). By comparing the results of these two models we can check the effect of slab size on our calculated results. Both models preserve inversion and reflection symmetry, which saves considerable computational effort. The self-consistent iteration is also stabilized by the enforcement of symmetry. The lattice constant of $BaTiO_3$ is set to the bulk value, which is 4.00 Å. The mismatch between metals and $BaTiO_3$ is given in Table I. Clearly, Ir and Pt have the smallest lattice constant mismatch (4% for Ir and 2% for Pt) and they are expected to grow epitaxially on the $BaTiO_3$ surface.

The electronic structure is treated in the framework of density-functional theory[9] in the local density-functional approximation[10] (LDA) and with the Hedin-Lundqvist[11,12] exchange-correlation potential. The highly precise full-potential linearized augmented plane-wave[13] (FLAPW) method is employed to solve the Kohn-Sham equations[10] self-consistently. In the FLAPW method, no shape approximations are made for the charge density, potential, and matrix elements. The core electrons are described by the atomic wave functions, which are solved fully relativistically in isolated atoms. The valence electrons are treated semirelativistically, i.e., the spin-orbit coupling is neglected.

Two energy windows, a valence panel and a semicore

TABLE I. Mismatch in metal/$BaTiO_3$ lattice constants.

Metal	Mismatch
Ta	21%
W	26%
Ir	4%
Pt	2%

TABLE II. Valence and semicore states in 5*d* metal/$BaTiO_3$.

Atom	Semicore	Valence
O	2*s*	2*p*
Ti	3*s*3*p*	4*s*3*d*
Ba	5*s*	5*p*6*s*
5*d* metal	5*p*	6*s*5*d*

panel, are used for the calculations and extended core levels such as Ti 3*p* are treated as semicore states, meaning that they are described by Bloch wave functions, not by atomic wave functions. Being in two different energy windows, the valence and semicore states are solved independently by ignoring their interactions. The setup of valence and semicore states is listed in Table II. We point out here that the O 2*s* and the metal 5*p* are put in the semicore panel because the repulsive force from their overlap plays an essential role in the interaction between O and metal. To get an equilibrium metal-oxygen distance, one has to orthogonalize these two states. The Ba 5*p* states are treated in the valence panel because they are close to the valence bands (at about 5 eV below the bottom of valence).

The muffin-tin (MT) radii of O, Ti, Ba, and the metals are set at 1.2, 2.1, 2.4, and 2.4 a.u., respectively. We use about 700 and 1700 plane waves to expand the electron wave functions in the interstitial region for the one-cell and three-cell models, respectively. The charge density and potential inside the MT spheres are expanded in spherical harmonics up to $l=8$ and 15 special k points in the 1/8 irreducible two-dimensional Brillouin zone are used to carry out the integrations.

III. INTERFACE STRUCTURE RESULTS

The equilibrium interfacial distances between metals and the $BaTiO_3$ (001) surface were determined by total-energy relaxation of the metal layer along the z direction. Three symmetric adsorption sites of the $BaTiO_3$ surface, i.e., above the O site, above the Ba site, and the hollow site, were investigated in the Pt/$BaTiO_3$ one-cell system to find out the most stable position for metal atoms. Figure 2 shows the total-energy relaxation for these three sites and one can see that the total energy of the O site is about 2.06 eV and 3.26 eV per unit cell lower than those of the hollow site and the Ba site, respectively. Therefore, the preferred adsorption site is above the O site. The Pt-O bond length for the O site, which is 2.12 Å (4.01 a.u.), is found to be smaller than the Pt-Ba bond length for the Ba site, which is 2.86 Å (5.40 a.u.). For the hollow site, the separation between the Pt layer and the $BaTiO_3$ surface is 1.97 Å (3.72 a.u.) and the corresponding Pt-O (or Pt-Ba) interatom distance is 2.83 Å (5.34 a.u.). One can also see from Fig. 2 that the total-energy relaxation curves of the Ba and hollow sites are flatter than for the O site. The large difference of binding energy and bond strength among these three adsorption sites may be due to the electrostatic interaction between Pt and the O or Ba ions since O and Ba carry a negative and a positive charge, respectively, in $BaTiO_3$ and the Pt nucleus is positively charged.

Due to the similarity among the 5*d* metals, we believe that the preferred adsorption site for Ta, W, and Ir is the same as for Pt, i.e., above the O site. The relaxation of the other transition metals above the O site on the $BaTiO_3$ surface were calculated with both one-cell and three-cell geom-

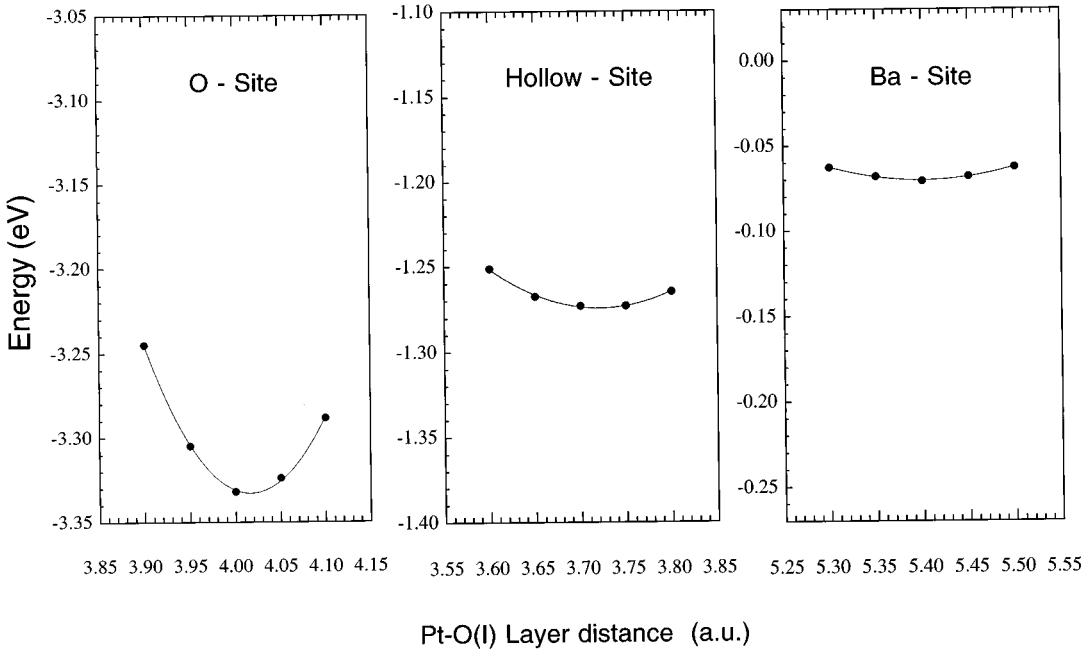

FIG. 2. Total energy vs distance between the Pt overlayer and the $BaTiO_3$ surface layer in the Pt/$BaTiO_3$ one-cell slab for three possible adsorption sites: Pt above the O site, Pt above the hollow site, and Pt above the Ba site.

TABLE III. Calculated metal-oxygen distances in metal/$BaTiO_3$ interfaces for one-cell and three-cell slabs with metal above the O site.

Metal	One-cell slab (Å)	Three-cell slab (Å)
Ta	2.04	2.05
W	2.07	2.07
Ir	2.13	2.11
Pt	2.12	2.11

etries; the calculated metal-oxygen distances are listed in Table III. Binding energies between metals and $BaTiO_3$ are listed in Table IV. As shown in Table III, the metal-oxygen distance increases from Ta to Pt because the smaller the atomic number, the weaker the Coulomb repulsive force between the metal core and O. Meanwhile, the interaction between Ta and O is stronger than between Pt and O because of the open shell atomic structure in Ta. Thus, as shown in Table IV, the binding energy decreases from Ta to Pt. Since the results of the metal-oxygen bond length from one-cell and three-cell models are in excellent agreement with each other, this implies that the interaction between metals and $BaTiO_3$ is limited to within less than two layers of the interface region.

IV. ELECTRONIC STRUCTURE AND INTERFACE INTERACTIONS

Charge transfer contours in the Pt/$BaTiO_3$ interface, obtained by subtracting the superposed charge density of the $BaTiO_3$ clean surface and the Pt monolayer from the Pt/$BaTiO_3$ charge density (all calculated self-consistently), are plotted along the (110) direction in Fig. 3. It is seen that the change of the charge density is localized in the interface area and that it decays rapidly into the $BaTiO_3$ bulk, which is consistent with the LAPW slab calculations for $BaTiO_3$ by Cohen.[14] Figure 3 demonstrates that the strong Coulomb repulsive potential of the O atom in the interface drives electrons away from the region between Pt and O. To calculate the charge transfer, we subtract the charge population of each atom in the metal monolayer or the clean $BaTiO_3$ surface from that in the interface and the results are listed in Table V. The charge in the metal atoms all increase by about 0.15 electron and the transfer to Ba, Ti, and O atoms is less than 0.06 electron. Such a small charge transfer indicates that therde is no strong ionic bonding between metals and $BaTiO_3$. More charge transfer in $BaTiO_3$ is found for Ta and W than for Ir and Pt.

As also demonstrated in Fig. 3, Pt electrons are moved from d_{z^2} states into $d_{x^2-y^2}$ states by the Coulomb repulsion

TABLE IV. Binding energies of metal/$BaTiO_3$ interfaces.

Metal	One-cell slab (eV/atom)	Three-cell slab (eV/atom)
Ta	5.58	5.45
W	5.35	4.96
Ir	4.97	4.73
Pt	4.23	3.90

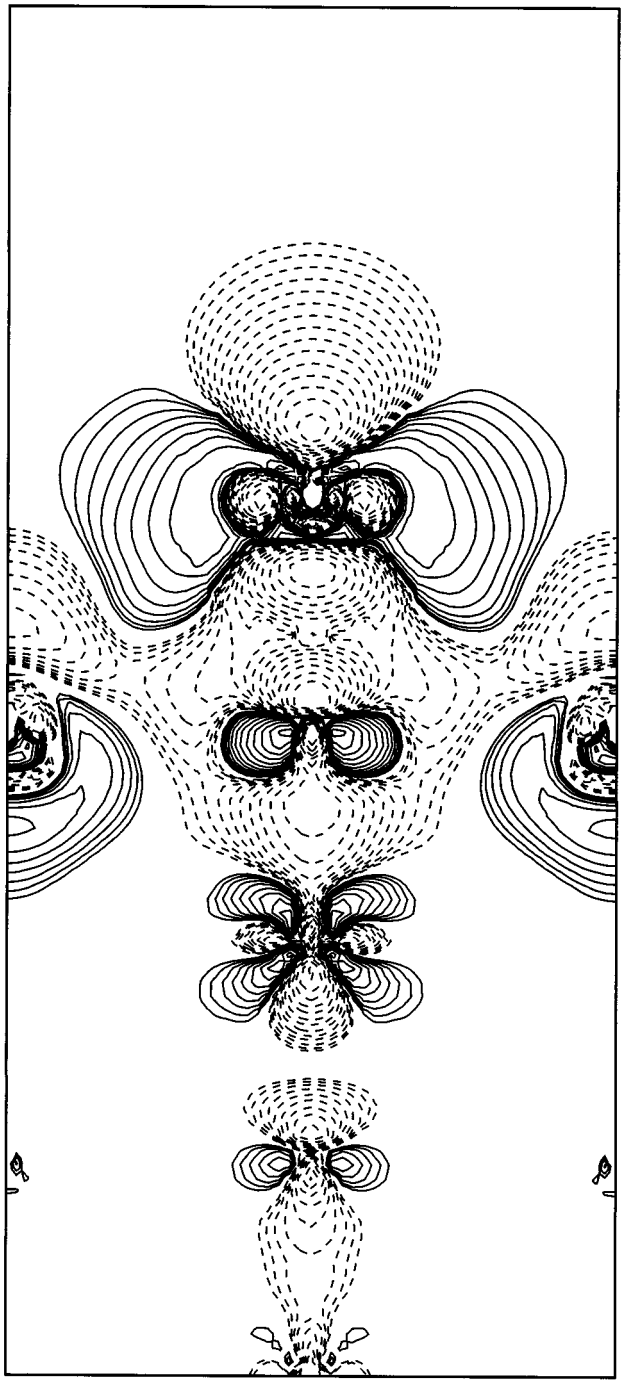

FIG. 3. Charge density difference, $\rho_{Pt/BaTiO_3}-\rho_{BaTiO_3}-\rho_{Pt\ ML}$ in the (110) plane. Solid lines denote electron accumulation and dashed lines denote electron loss. Contours start from $\pm 5\times10^{-4}$ electrons/a.u.^{3} and change successively by a factor of $\sqrt{2}$.

of the O $2p$ electrons. With less d_{z^2} character, the Pt layer has less electron spill out into the vacuum so the dipole moment between Pt and vacuum is reduced. Consequently, the Coulomb barrier from Pt to vacuum is lowered and the Pt work function decreases from 6.47 eV in the free monolayer to 4.71 eV in the overlayer. The calculated work functions of other metals in both the monolayer (all with the same lattice constant as $BaTiO_3$) and interface, as well as the work function of the $BaTiO_3$ clean surface, are listed in Table VI. We found that the 5d metal work function increases with atomic

TABLE V. Charge transfer for metal/$BaTiO_3$ three-cell slabs calculated as differences of charge populations in muffin-tin spheres between the $BaTiO_3$ clean surface or the free metal monolayer and the interface.

Metal	Metal	O(I)	Ba(I)	O(I-1)	Ti(I-1)	O(I-2)	Ba(I-2)	O(C)	Ti(C)
Ta	0.133	0.028	0.053	−0.003	0.028	−0.004	−0.003	−0.002	0.015
W	0.162	0.022	0.048	−0.002	0.019	−0.004	−0.003	−0.001	0.011
Ir	0.155	0.004	0.027	−0.002	0.002	−0.003	−0.002	−0.001	−0.001
Pt	0.150	0.002	0.022	−0.002	−0.001	−0.002	−0.002	−0.001	−0.001

number from Ta to Pt in both the free monolayer and interface cases. For all the other metals, work functions for the overlayers are lower than for the free monolayers, but higher than for the $BaTiO_3$ surface.

The partial density of states (DOS) projected on each atom in the three-cell $BaTiO_3$ clean surface and the free Pt monolayer are plotted in Fig. 4. The $BaTiO_3$ valence bands lie from the Fermi energy (E_F) to about 5 eV below (the tails of the valence bands above E_F come from the broadening of the plot). The Ti DOS shows that the valence states have significant weight on the Ti ions and so they are hybridized O 2p–Ti 3d states instead of pure O 2p states. Ba is essentially fully ionized with a very low DOS in the valence region. The lower part of the conduction bands are mainly the Ti 3d states. Because of the reduced number of neighboring atoms at the surface, the O(S) 2p bands are narrower and sharper than those of the other O layers. For comparison, we have also carried out calculations for bulk $BaTiO_3$ and plot the DOS of the O, Ti, and Ba atoms in bulk $BaTiO_3$ by dashed lines in Fig. 4 together with the O(C), Ti(C), and Ba(S-2) densities of states, respectively. It is clear that the DOS of the S-2 and central layers recover bulklike features, while the S-1 and surface layers show different structures compared with the bulk. The calculated gap of the three-cell $BaTiO_3$ clean slab is 1.22 eV. This number is quite close to the calculated bulk value, which is 1.16 eV. For the one-cell $BaTiO_3$ slab, the calculated gap is 1.39 eV. With ionic bonding in $BaTiO_3$, electrons are localized around nuclei and the size effect on the gap is expected to be insignificant in the thicker slab. These results are in agreement with the LAPW slab calculations.[14] As usual in LDA calculations, the computed gap value is smaller than the experimental value, which is about 3.13 eV.[28]

The partial DOS of three-cell Pt/$BaTiO_3$ with Pt above the O site is plotted in Fig. 5. Significant hybridization features are found between the Pt 5d and O 2p states. Com-

TABLE VI. Calculated work functions of metals in free monolayers and metal/$BaTiO_3$ interfaces (one-cell and three-cell slabs). The lattice constant of free metal monolayers are the same as $BaTiO_3$. For comparison, the work functions of the clean $BaTiO_3$ surfaces are also listed.

Metal	ML (eV)	One-cell slab (eV)	Three-cell slab (eV)
Ta	4.68	3.55	3.55
W	5.32	4.01	4.03
Ir	6.29	4.82	4.88
Pt	6.47	4.87	4.71
$BaTiO_3$		3.42	3.22

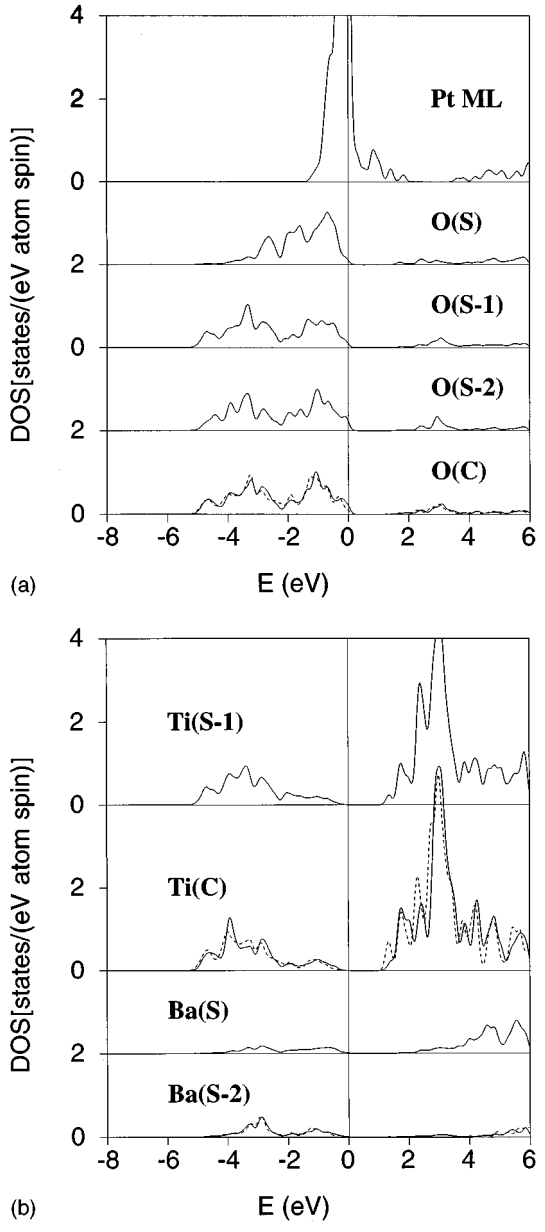

FIG. 4. Partial density of states (DOS) projected on the muffin-tin spheres of (a) Pt and O and (b) Ti and Ba in the free Pt monolayer and the three-cell $BaTiO_3$(001) clean surface. For comparison, the DOS of the O, Ti, and Ba atoms in the $BaTiO_3$ bulk are plotted by dashed lines together with the O(C), Ti(C), and Ba(S-2) densities of states. The Fermi energy is set at zero. The tails of the $BaTiO_3$ valence bands above E_F come from the broadening of plotting.

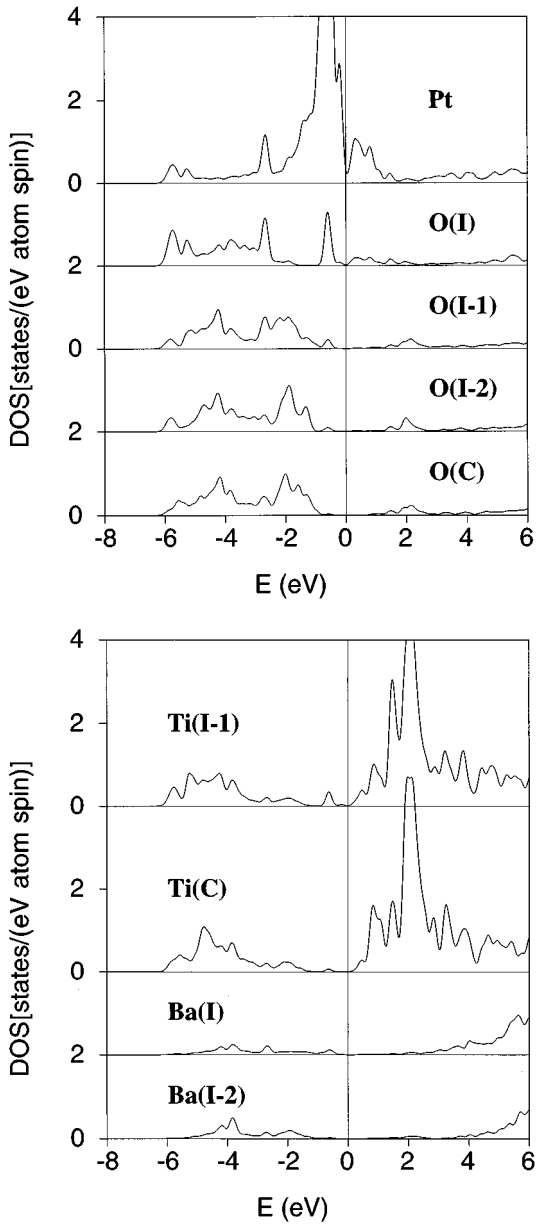

FIG. 5. Partial density of states projected on the muffin-tin spheres of Pt and O (upper panel) and Ti and Ba (lower panel) in the three-cell Pt/$BaTiO_3$ interface with Pt above the O site. The Fermi energy is set at zero.

pared to the free Pt monolayer, new peaks are developed in the Pt overlayer from about 2.0–5.8 eV below E_F with an almost identical structure in the O(I) layer. The main Pt 5d peak is broadened by the interaction with O and the peak height drops from about 19 states/(eV atom spin) in the free monolayer to about 14 states/(eV atom spin) in the overlayer. The density of states at E_F for Pt (or other metals) drops dramatically from about 15 states/(eV atom spin) to about 0.4 states/(eV atom spin). In the O(I) DOS, a sharp peak is formed by the tail of Pt 5d states right in the gap region at about 0.6 eV below E_F and it penetrates to the O(I-2) and Ti(I-2) atoms. Two peaks near the bottom of the valence bands at about 5.7 eV and 5.2 eV below E_F are strongly enhanced in O(I), whereas they actually vanish in the clean surface case. The DOS of atoms in the two central layers remain basically unchanged. Similar hybridization features are also found in the interfaces between $BaTiO_3$ and other transition metals.

V. SCHOTTKY BARRIERS

The Schottky barrier is formed in metal-semiconductor or metal-insulator interfaces between the metal Fermi level and the bottom of the semiconductor (or insulator) conduction bands.[15] The barrier height depends on the position of the metal Fermi energy in the interface. It can be shown that in any metal-insulator (or metal-semiconductor) interface, the metal E_F has to stay within the insulator gap region to balance charge populations on both sides. Otherwise electrons will transfer from bulk insulator valence states to metal states (if E_F lies below the gap) or from metal to bulk insulator conduction states (if E_F is above the gap). Because the bulk states are all extended states, this transfer must happen everywhere in the volume of the insulator. Therefore, the metal and insulator will be unphysically polarized even far away from the interface. When E_F lies in the gap, since for energies in the band gap the metal states decay exponentially into the insulator side due to lack of matching insulator bulk state at the same energy,[16–18] the charge transfer is confined within a few atomic layers in the interface and the electron occupation in the bulk is unaffected. Thus, as a result of charge balance, the only place the metal Fermi level can stay in metal-insulator interfaces is inside the gap.

For the transition metal/$BaTiO_3$ interface, from the O(C) density of states in Fig. 5(a), one can see that the Pt Fermi energy lies in the gap of $BaTiO_3$ at about 1.0 eV above the bottom of the gap. Notice that as shown in Table IV, E_F of the free Pt monolayer is located at 6.47 eV below the vacuum potential and the top of the valence bands in the clean $BaTiO_3$ three-cell slab is located at 3.22 eV below vacuum. So the Pt E_F is 3.25 eV below the bottom of the gap when Pt and $BaTiO_3$ are separated. After Pt is deposited on the $BaTiO_3$ surface, electrons are transferred from $BaTiO_3$ to Pt by the interfacial hybridization. A dipole layer is then formed between Pt and $BaTiO_3$ in the interface to raise the Pt Fermi level relative to the $BaTiO_3$ bands until it moves into the gap. Actually, for all the other 5d metals, E_F is shifted from below the gap to inside the gap by the dipole layer in the interfaces. The tail of the metal 5d states in $BaTiO_3$, recognized as metal-induced gap states (MIGS's), appears clearly in the O(I) layer.

The effect of the metal-induced gap states was pointed out by Heine[19] and discussed by a number of authors.[20–27] In Heine's theory, the metal-induced gap states transfer metal electrons into the semiconductor (or insulator) in the metal-semiconductor (or insulator) system. The shift of E_F is determined by the mismatch of work functions between the metal and the semiconductor (or insulator), the dielectric constant in the interface, the density of states, and the penetration length of the MIGS's in the semiconductor (or insulator). For a more general case, the E_F shift is controlled by both the MIGS's and the tail of the semiconductor (or insulator) valence states. As shown in Fig. 5(a), the $BaTiO_3$ valence states below the Pt 5d bands also penetrate into the Pt side by the same mechanism as MIGS's and cause the charge transfer from $BaTiO_3$ to Pt. Finally, the position of

TABLE VII. Energy differences between the metal Fermi energy (E_F) and the top of the $BaTiO_3$ valence bands (E_v) in the metal/$BaTiO_3$ interface determined by the central layer density of states in three-cell slabs. The Schottky barrier (ϕ_b) is calculated by subtracting E_F-E_v from the experimental gap value of $BaTiO_3$ (3.13 eV) (Ref. 28).

Metal	E_F-E_v (eV)	ϕ_b (eV)
Ta	1.19	1.94
W	1.13	2.00
Ir	0.64	2.49
Pt	0.94	2.19

E_F is determined by the balance between these two processes.

First-principles calculations of the Schottky barrier at interfaces of aluminium and Si, Ge, GaAs, ZnSe, and ZnS semiconductors were carried out by Cohen and coworkers.[21–23] In a similar approach to theirs, we extrapolate the position of E_F in the gap from the partial density of states of the central layer in the metal/$BaTiO_3$ three-cell slab where the band gap is well defined. The calculated energy differences between the Fermi energy and the top of the $BaTiO_3$ valence bands (E_F-E_v) are listed in Table VII. We also estimate the Schottky barrier height ϕ_b by subtracting E_F-E_v from the experimental gap value $E_{\rm gap}^{\rm expt}$ (3.13 eV) (Ref. 28) as

$$\phi_b=E_{\rm gap}^{\rm expt}-(E_F-E_v). \tag{1}$$

The results are listed in Table VII. The position of the 5*d* metal E_F in the gap shows a descending trend from Ta to Pt except for Ir, which has a lower E_F than Pt. Table VII shows that E_F at the interface changes significantly for the different metals. No Fermi energy pinning, which was suggested by Bardeen,[29] is observed in these transition-metal/$BaTiO_3$ interfaces. This is in agreement with the observation of Louie *et al.*[23] that the Schottky barrier is much less dependent on the metal for the covalent materials than for the ionic ones. It is believed that the barrier height is a monotonic function of the free metal work function W_m and, under the Schottky-Mott limit, ϕ_b is simply a linear function of W_m. To check this, we plot ϕ_b vs the free metal monolayer work function W_m in Fig. 6. Apparently ϕ_b does not vary monotonically with W_m in the transition-metal/$BaTiO_3$ interfaces (not with the measured metal work function $W_m^{\rm expt}$ either since $W_m^{\rm expt}$ increases from Ta to Pt) and the Schottky barrier is determined by the details of the interfacial interactions.

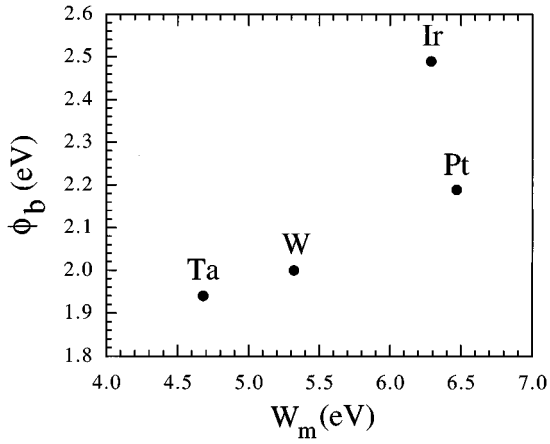

FIG. 6. Schottky barrier (ϕ_b) vs the free metal monolayer work function (W_m).

VI. SUMMARY

In summary, we have investigated the structural and electronic properties of some 5*d* transition-metal/$BaTiO_3$ interfaces by first-principles calculations. The adsorption site for the metal atoms on the $BaTiO_3$(100) surface is above the O site. The interfacial distance is found to increase from Ta to Pt for the metals, while the binding energy is found to decrease, which shows a stronger binding in Ta and W than in Ir and Pt. The 5*d* metal Fermi energy is moved by the interface dipolar potential from below the $BaTiO_3$ gap in the monolayer to inside the gap at the interface to balance the charge in each side. The Schottky barrier between the metal and $BaTiO_3$ is calculated according to the position of E_F in the gap. Despite the gap problem of LDA calculations, we are able to estimate the relative barrier height and to give the trend among different metals in such an approach. Because of the effects of the Schottky barrier on the DRAM performance, such as leakage current and breakdown field, it is important to understand the formation of the Schottky barrier at the metal/ferroelectric interfaces and the dependence of the barrier height on the metals. For the transition-metal/$BaTiO_3$ interfaces, our calculations show that neither Schottky and Mott's nor Bardeen's speculation can explain the behavior of the barrier height and that Heine's picture of the metal-induced gap states is supported by the interface electronic structures.

ACKNOWLEDGMENTS

This work is supported by the U.S. Department of Energy (Grant No. DE-FG02-88ER45372) and by a grant of computing time on the NERSC supercomputers.

[1] *The National Technology Roadmap for Semiconductors* (Semiconductor Industry Association, San Jose, CA, 1994), pp. 11 and 16.

[2] Y. Ohno, T. Horikawa, H. Shinkawata, K. Kashinhara, T. Kuroiwa, T. Okudaira, Y. Hashizume, K. Fukumoto, T. Eimori, T. Shibano, K. Arimoto, H. Itoh, T. Nishimura, and H. Miyoshi, *Digest of Technical Papers—Symposium on VLSI Technology 1994* (IEEE, Piscataway, 1994), pp. 149 and 150.

[3] R. Khamankar, B. Jiang, R. Tsu, W. Hsu, J. Nulman, S. Summerfelt, M. Anthony, and J. Lee, *Digest of Technical Papers—Symposium on VLSI Technology 1995* (IEEE, Piscataway, 1995), pp. 127 and 128.

[4] X. Chen and A. I. Kingon, in *Proceedings of the IEEE International Symposium on Applied Ferroelectrics, Greenville, SC, 1992*, edited by S. T. Liu (IEEE, Piscataway, 1992), paper 3C-6, p. 75.

[5] J. F. Scott, M. Azuma, C. A. Paz de Araujo, L. D. McMillan, M. C. Scott, and T. Roberts, Integrated Ferroelectrics **4**, 61 (1994).
[6] K. Abe and S. Komatsu, Jpn. J. Appl. Phys. **32**, 4186 (1993).
[7] J. Kim, R. Khamankar, C. Sudhama, B, Jiang, J. Lee, S. Summerfelt, and B. Gnade (unpublished).
[8] G. W. Dietz, W. Antpohler, M. Klee, and R. Waser, J. Appl. Phys. **78**, 6113 (1995).
[9] P. Hohenberg and W. Kohn, Phys. Rev. **136**, B864 (1964).
[10] W. Kohn and L. J. Sham, Phys. Rev. **140**, A1133 (1965).
[11] U. Von Barth and L. Hedin, J. Phys. C **5**, 1629 (1972).
[12] L. Hedin and B. I. Lundqvist, J. Phys. C **4**, 2064 (1971).
[13] E. Wimmer, H. Krakauer, M. Weinert, and A. J. Freeman, Phys. Rev. B **24**, 864 (1981), and references therein.
[14] R. E. Cohen, J. Phys. Chem. Solids **57**, 1393 (1971).
[15] See, e.g., E. H. Rhoderick and R. H. Williams, *Metal-Semiconductor Contacts*, 2nd ed. (Oxford University Press, London, 1988).
[16] V. Heine, Proc. Phys. Soc. London **81**, 300 (1962).
[17] P. J. Price, *Report of the International Conference on the Physics of Semiconductors* (Institute of Physics and the Physical Society, London, 1962), p. 99.
[18] V. Heine, Surf. Sci. **2**, 1 (1964).
[19] V. Heine, Phys. Rev. **138**, A1689 (1965).
[20] F. Yndurain, J. Phys. C **4**, 2849 (1971).
[21] S. G. Louie and M. Cohen, Phys. Rev. Lett. **35**, 866 (1975).
[22] S. G. Louie and M. Cohen, Phys. Rev. B **13**, 2461 (1976).
[23] S. G. Louie, J. R. Chelikowsky, and M. Cohen, Phys. Rev. B **15**, 2154 (1977).
[24] C. Tejedor, F. Flores, and E. Louis, J. Phys. C **10**, 2163 (1977).
[25] J. Ihm, S. G. Louie, and M. Cohen, Phys. Rev. B **18**, 4172 (1978).
[26] J. Tersoff, Phys. Rev. Lett. **52**, 465 (1984).
[27] J. Tersoff, Phys. Rev. B **32**, 6968 (1985).
[28] H.-J. Hagemann and D. Hennings, J. Am. Ceram. Soc. **64**, 590 (1981).
[29] J. Bardeen, Phys. Rev. **71**, 717 (1947).